Crystal structure of glycoprotein C from Rift Valley fever virus

Moshe Dessau and Yorgo Modis[1]

Department of Molecular Biophysics and Biochemistry, Yale University, New Haven, CT 06520

Rift Valley fever virus (RVFV), like many other *Bunyaviridae* family members, is an emerging human and animal pathogen. Bunyaviruses have an outer lipid envelope bearing two glycoproteins, G_N and G_C, required for cell entry. Bunyaviruses deliver their genome into the host-cell cytoplasm by fusing their envelope with an endosomal membrane. The molecular mechanism of this key entry step is unknown. The crystal structure of RVFV G_C reveals a class II fusion protein architecture found previously in flaviviruses and alphaviruses. The structure identifies G_C as the effector of membrane fusion and provides a direct view of the membrane anchor that initiates fusion. A structure of nonglycosylated G_C reveals an extended conformation that may represent a fusion intermediate. Unanticipated similarities between G_C and flavivirus envelope proteins reveal an evolutionary link between the two virus families and provide insights into the organization of G_C in the outer shell of RVFV.

icosahedral lattice assembly | parallel evolution | pH sensing | prehairpin

The *Bunyaviridae* are a large and diverse family of human, animal, and plant pathogens present worldwide. Rift Valley fever virus (RVFV) was isolated in 1930 in Kenya and has since become a medically and agriculturally important virus across Africa and the Arabian peninsula (1). Humans can be infected by a bite from *Aedes* (2) or various other species (3) of mosquito, but RVFV is also highly infectious by contact and aerosol, and most infections result from contact with infected livestock (1). Along with the spread of *Aedes* mosquitos into Europe and the Americas (4), efficient aerosol transmission of RVFV raises concerns of further expansion of the endemic zones. Moreover, recently discovered viruses belonging to the same phlebovirus genus as RVFV have been associated with lethal human diseases (5, 6).

To deliver their three single-stranded negative- and ambisense RNA genome segments into the cytoplasm, bunyaviruses must fuse their envelope with a cellular membrane. Other enveloped viruses such as influenza virus, with its prototypical class I hemagglutinin fusion protein, or flaviviruses, with their prototypical class II envelope (E) glycoproteins, typically enter the endocytic pathway following cellular attachment. The glycoproteins respond to the reduced pH of endocytic compartments with a conformational change that exposes a hydrophobic fusion peptide or fusion loop allowing it to insert into the endosomal membrane. The glycoproteins then fold back on themselves, forcing the cell membrane (held by the fusion loop) and the viral membrane (held by a transmembrane anchor) against each other, resulting in fusion of the viral and endosomal membranes (7–9). Bunyaviruses appear to use a similar cell entry mechanism. Following cellular attachment they enter the endocytic pathway (10). The two glycoproteins of RVFV, G_N and G_C, assemble around the lipid envelope in which they are anchored into an icosahedral $T = 12$ lattice, forming a rigid outer protein shell with an average diameter of 103 nm (11, 12). The ability of viruses and virus-like particles in the family to mediate syncytia formation at low pH provides indirect support for endosomal membrane fusion as a mode of entry (13, 14). The Uukuniemi phlebovirus undergoes acid-activated membrane fusion in late endosomal compartments with a pH threshold of 5.4 (10). Based on proteomic and computational analyses, it has been postulated that bunyavirus G_C proteins mediate fusion and are class II viral fusion proteins (15, 16). This is supported experimentally by the interaction of the putative fusion loop of a hantavirus G_C protein with artificial membranes (17). Moreover, proteolytic

assays, detergent partitioning experiments, and antibody binding studies suggest that the G_C of orthobunyaviruses undergoes a conformational change at low pH (18). In the absence of experimental structural data for G_C, the molecular basis of membrane fusion in bunyaviruses has remained unclear. We have determined the crystal structure of the RVFV G_C ectodomain truncated 41 residues before its C-terminal transmembrane helix (M polyprotein residues 691–1,119).

Results and Discussion

RVFV G_C Is a Class II Membrane Fusion Protein. The structure of RVFV G_C, refined at 1.9-Å resolution (Table 1), reveals a three-domain class II fusion protein fold in the prefusion form, found previously only in flaviviruses and alphaviruses (19–21) (Fig. 1 *A* and *B*). This class II fold definitively identifies G_C as the effector of membrane fusion in phleboviruses. Domain I, a 10-stranded β-barrel, organizes the structure. A 3-stranded sheet is appended onto extensions of the fifth and sixth barrel strands. Two insertions in domain I form the elongated, mostly β-stranded domain II. Domain III is an IgC-like module with 7 β-strands. The overall configuration bears strong similarity (22) to alphavirus E1 proteins and flavivirus E proteins (Fig. 1 *C* and *D*) despite the highly divergent sequence of RVFV G_C relative to these other class II proteins (Fig. S1).

Among the notable differences between RVFV G_C and other class II proteins, the interface between domains I and II is more extensive and may be more rigid than in other class II proteins. The fifth and sixth β-strands of domain I extend into domain II and merge with strands that in other class II proteins form part of a separate β-sheet in domain II. This β-sheet, packs against the aforementioned three-stranded extra sheet on domain I and a hairpin structure analogous to the kl-hairpin in flavivirus E (21) to form a small β-barrel straddling the boundary between domains I and II (Fig. 1*B*). We note that this β-barrel has a hydrophobic core that could conceivably accommodate a hydrophobic ligand as can dengue E (21) (Fig. S2). Together these features suggest that the domain I–II boundary may be more rigid than in other class II proteins, in which it acts as a hinge during membrane fusion (8, 21). Other specific properties of RVFV G_C are the larger number of disulfide bonds than other class II proteins (12 versus 6 or 7) and the different positions of the disulfide bonds and glycans (Fig. 1 *B–D* and Fig. S1*A*). Moreover, the oligosaccharide chain on Asn1035 in domain III extends across the interface between domains I and III, forming contacts with domain I (Fig. 1*B*).

Structure of the Putative Fusion Loop Membrane Anchor. The RVFV G_C structure provides a direct view of the putative fusion loop, which can be clearly identified by analogy to other class II proteins as spanning residues 820–830. The fusion loop has a tightly folded conformation stabilized by two disulfide bonds

Table 1. Crystallographic data collection and refinement statistics

Dataset	Native	Os	Tunicamycin
Data collection			
Space group	$P2_1$	$P2_1$	$P6_422$
Cell dimensions			
a, b, c, Å	128.7, 56.4, 140.2	69.5, 57.0, 129.9	114.3, 114.3, 170.7
α, β, γ (°)	90, 96.6, 90	90, 99.6, 90	90, 90, 120
Wavelength, Å	0.9795	1.1398	1.1
Resolution, Å*	30–1.8 (1.95–1.9)	30–3.0 (3.15–3.0)	40–4.15 (4.22–4.15)
Unique reflections	154,051	38,015	5,438
R_{merge}, %*,†	7.2 (99.9)	18.6 (93.1)	7.5 (99.9)
$I/\sigma I$*	10.3 (1.4)	5.2 (1.6)	31.6 (1.4)
Completeness, %*	97.4 (85.6)	96.6 (98.2)	99.8 (100)
Redundancy*	3.88 (3.0)	2.55 (2.6)	12.6 (13.5)
Overall figure of merit		0.45	
Refinement			
Resolution, Å	30–1.9		20–4.15
No. reflections	146,309		5,331
R_{work}/R_{free}, %‡	21.3/25.6		25.9/31.1
Averaged B factor, Å²§	62.1		159.5
RMS deviations			
Bond lengths, Å	0.009		0.004
Bond angles (°)	1.4		0.8
Ramachandran analysis			
Preferred regions, %	96.7		93.4
Allowed regions, %	3.0		6.1
Disallowed regions, %	0.3		0.5
Synchrotron beamline	APS NE-CAT 24ID-C	APS NE-CAT 24ID-C	BNL X25

RMS, root mean square.
*Highest resolution shell is shown in parentheses.
†$R_{sym} = \Sigma_{hkl}\Sigma_i \, |I_{hkl,i} - <I>_{hkl}|/\Sigma_{hkl}\Sigma_i|I_{hkl,i}|$, where I_{hkl} is the intensity of a reflection and $<I>_{hkl}$ is the average of all observations of the reflection.
‡R_{free}, R_{work} with 10% of F_{obs} sequestered before refinement.
§Residual B-factors after TLS refinement. See PDB ID code for TLS refinement parameters.

(Fig. 1E). The G_C fusion loop is remarkably similar to flavivirus E fusion loops (20, 21), including the composition of the amino acids that serve as membrane anchors: Trp821, Phe826, Val828 in G_C versus Trp101, Leu107, and Phe108 in dengue E (Fig. 1E). We note that Leu779, on an adjacent loop and in van der Waals contact with Phe826, extends the fusion loop's hydrophobic surface and may thus participate in membrane anchoring. The requirement for detergent in the crystallization solution (*Materials and Methods*) provides circumstantial evidence that G_C contains exposed hydrophobic surfaces.

Location of Proposed pH-Sensing Histidine Side Chains. Histidine side chains have pK_a values in the range of 6–6.4 and therefore typically become protonated during endosomal acidification. The increase in positive charge resulting from histidine protonation is an important part of the pH sensing mechanism of alphaviruses and flaviviruses. Protonation of conserved histidines at the domain I–domain III interface of alphavirus and flavivirus envelope proteins triggers the fusogenic conformational change by destabilizing the prefusion conformation and stabilizing the postfusion conformation of the protein (23–26). Notably, a recent study showed that three conserved histidine residues in RVFV G_C, His778, His857, and His1087, are required for virus infectivity (27). The position of His1087 in domain III is analogous to the position of His323 in tick-borne encephalitis (TBE) E or His317 in dengue E. This is the most critical histidine in flavivirus E proteins for both the initiation and propagation of the fusogenic conformational change (23, 24). Although His1087 does not form contacts with domain I in G_C, in contrast to His317/323 in E, protonation of His1087 may still alter the thermodynamic landscape in favor of membrane fusion, for example by stabilizing the postfusion conformation of G_C. His778 is adjacent to the putative membrane-anchoring residue Leu779 (see above) and to the fusion loop. Protonation of His778 may

stabilize interactions with the phosphate moieties of lipid headgroups. His857 is buried inside domain I, forming hydrogen bonds with the side chains of Asp893 and Ser752. Protonation of His857 is not expected to destabilize either of these interactions and it is unclear from the structure of G_C how His857 might serve as a pH sensor. The failure of a H857A mutant virus to form acid-induced G_C SDS-resistant oligomers and the location of His857 at the core of domain I suggest that His857 may serve a purely structural role rather than a pH-sensing role.

Nonglycosylated RVFV G_C Crystallized in a Prehairpin-Like Conformation. The N-linked glycan on G_C from Hantaan virus is required for membrane fusion activity (14). We found that RVFV G_C expressed in the presence of tunicamycin, an N-glycosylation inhibitor, crystallized in a different conformation than glycosylated G_C. The most salient difference of the structure, refined at 4.1 Å resolution, is a 91° rotation of domain III relative to domain I compared with the glycosylated structure (Fig. 2A). Domain III also has higher temperature factors in the nonglycosylated structure, suggesting a degree of flexibility, possibly due to the lack of stabilizing oligosaccharide-mediated contacts between domains I and III. Domain II is rotated relative to domain I by 4° in non-glycosylated G_C. Because of these differences, nonglycosylated G_C is in a more extended conformation, spanning 160 Å. With the fusion loop and the C terminus located at opposite ends of the protein, this extended conformation is likely to correspond to the so-called prefusion or prehairpin intermediate postulated (but not directly observed) for all fusion proteins, in which the protein bridges the cellular and viral membranes, with its fusion loop bound to the former and its transmembrane tail anchored in the latter (8, 28) (Fig. S3). Because the fusogenic transition of class II proteins relies on hinge-like motions at both domain interfaces (8, 9), the domain rotations observed between the two G_C crystal structures
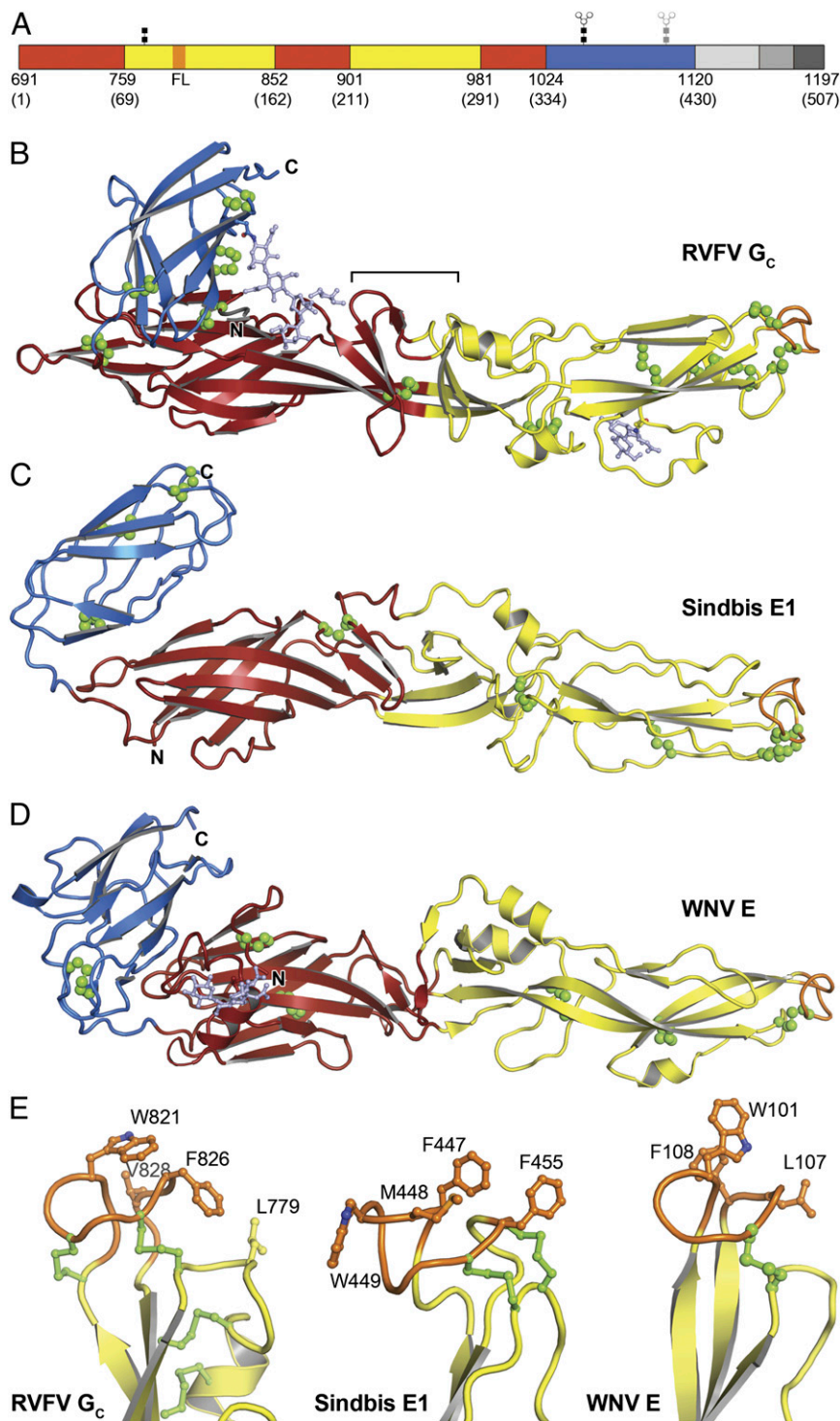
Fig. 1. Overall fold of RVFV G_C and comparison with other class II membrane fusion proteins. (*A*) RVFV G_C has the same three-domain architecture as other class II proteins. Domain I is in red, domain II is in yellow with the fusion loop in orange, and domain III is in blue. Residue numbers follow M-segment polyprotein numbering, with corresponding G_C residue numbers in parentheses. In the structure, (*B*), the stem region (light gray), transmembrane anchor (medium gray), and cytoplasmic tail (dark gray) are missing. Glycans are linked to N794, N1035 (light blue), and N1077 (gray, disordered in the structure). The β-barrel connecting domains I and II is marked with a bracket. Disulfide bonds are in green. (*C*) Structure of Sindbis virus glycoprotein E1 [PDB ID code 3MUU (33), the most similar alphavirus envelope protein, with a Z-score of 15.1 in Dali (42). (*D*) Structure of West Nile virus glycoprotein E [PDB ID code 2I69 (30)], the most similar flavivirus glycoprotein, with a Z-score of 13.3. (*E*) The putative fusion loop of RVFV G_C and the fusion loops of Sindbis E1 and West Nile E. The hydrophobic residues that anchor the protein to the cellular membrane and the disulfide bonds are shown in ball-and-stick representation.

are consistent with G_C catalyzing membrane fusion with a similar conformational change to other class II proteins.

Glycosylated RVFV G_C Forms Dimers in the Crystal Similar to Flavivirus E Dimers. Although the RVFV G_C ectodomain is a monomer in solution at neutral and acidic pH (Fig. S4), G_C forms two identical dimers per asymmetric unit in the crystal. The head-to-tail configuration of the dimers is strikingly similar to that of flavivirus E dimers, with the fusion loop buried at the dimer interface (Fig. 2*B*). Moreover, a glycan extends laterally across the G_C dimer interface and covers the fusion loop of the dimer partner, as in the

TBE E dimer (20). The solvent-inaccessible surface area within the G_C dimer interface is similar (12–15% smaller) to those of flavivirus E dimers. The fusion loop and surrounding region of G_C form more extensive dimer contacts, including notably a π-stacking interaction between the side chains of Trp821 in the fusion loop and Arg1047 in domain III of the dimer partner (Fig. 3). The other side of the Trp821 side chain forms an intramolecular van der Waals interaction with Phe826, in the fusion loop. The larger number of dimer contacts involving the fusion loop in G_C may increase the energy barrier for exposure of the fusion loop, which is consistent
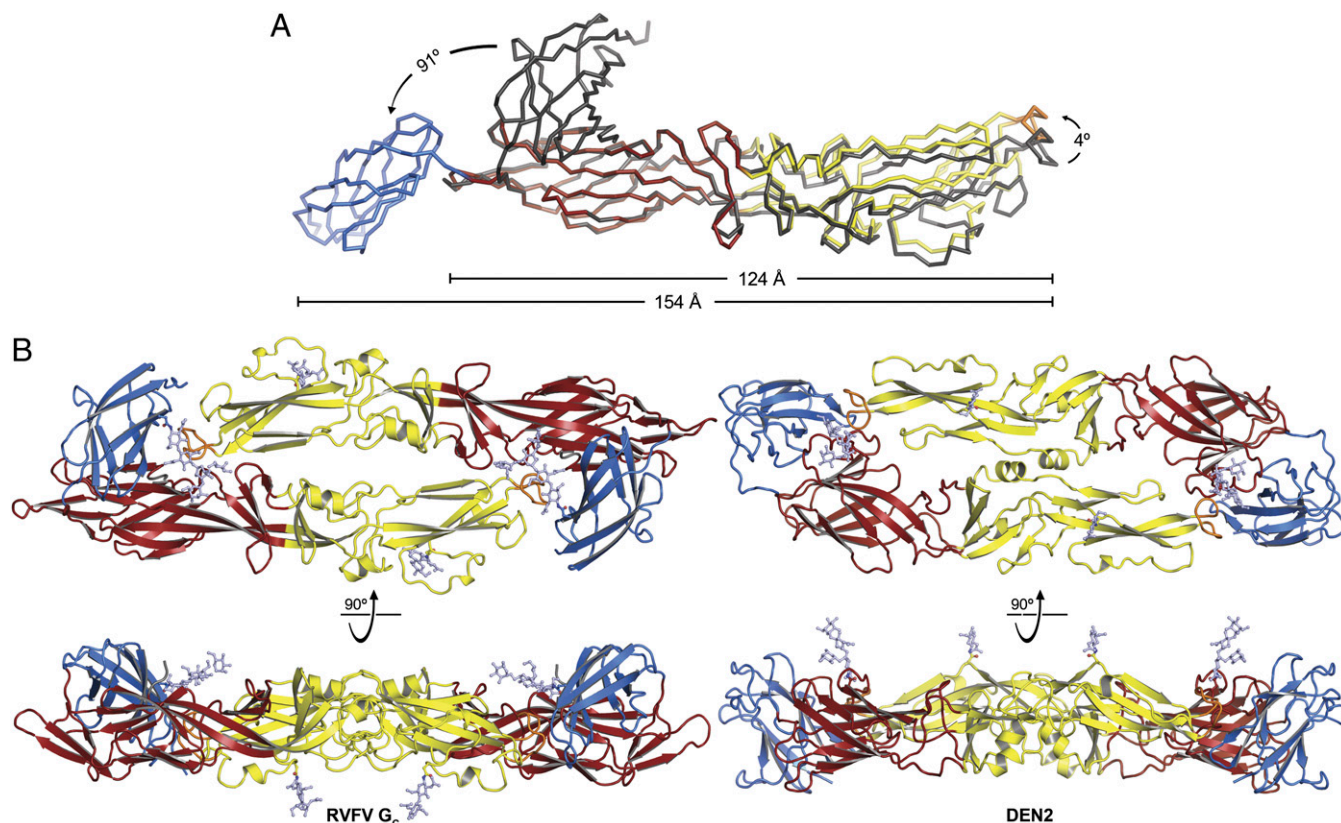
Fig. 2. Nonglycosylated RVFV G_C has an extended conformation and glycosylated G_C forms a head-to-tail dimer in the crystal. (*A*) The structure of non-glycosylated G_C, colored as in Fig. 1, with glycosylated G_C (gray) superimposed using domain I as the reference. Arrows show the hinge motions of domains II and III relating the two structures. See also Fig. S3. (*B, Left*) RVFV G_C dimer. The overall arrangement closely resembles that of E proteins in mature flaviviruses and in crystal structures. (*Right*) E dimer from dengue type 2 virus [PDB ID code 1OAN (21)].

with the lower pH threshold of fusion for phleboviruses [5.4 (10) versus ~6.3 for flaviviruses (29)].

Nonglycosylated G_C does not form the same dimer in the crystal, but this is not surprising given the different conformation and increased flexibility of domain III in the absence of glycan-mediated contacts with domain I (Fig. 2). However, nonglycosylated G_C forms extensive packing contacts around a crystallographic two-fold symmetry axis (Fig. S3). The resulting crystallographic dimer has a buried surface area nearly half that of the glycosylated dimer, large enough to suggest that the dimers represent a metastable intermediate in the fusion transition.

Nature of the Evolutionary Link Between Class II Fusion Proteins. The similarity of the RVFV G_C dimer to flavivirus E dimers and the extent of the dimer interface, with the fusion loop shielded from the solvent as would be expected in a prefusion conformation, suggest that the G_C dimer is physiological rather than a crystallization artifact. Indeed, various flavivirus E proteins are monomeric in solution but form dimers in the crowded environment of the outer protein shell of the virus or of a protein crystal (30, 31). The class II fold of G_C and the striking structural similarity of the G_C and E dimers are strongly suggestive of an evolutionary link between *Bunyaviridae* and *Flaviviridae*. However, what is the nature of this link? The two virus families clearly differ in their genomic organization, coding strategies, and outer protein shell assemblies (12, 32–34). In light of these differences, it is tempting to speculate that, rather than diverging from a common ancestor virus, class II fusion proteins may instead have evolved independently from a common and as yet unidentified ancestral cellular class II membrane fusion protein.

Organization of G_C Within the Outer Protein Shell of RVFV. The outer shell of flaviviruses is assembled from 90 E dimers in an unusual herringbone icosahedral configuration with three distinct, non-equivalent packing environments for E (32). Electron microscopy (EM) of RVFV shows that it has a more common quasiequivalent icosahedral symmetry with penta- and hexavalent capsomers (11, 12). The G_C dimer could not be fitted into the 22 Å-resolution EM structure of RVFV with the dimer dyad axis perpendicular to the viral surface as in flaviviruses without major steric clashes. The only way to fit the G_C dimer into the EM structure without clashes and within the icosahedral symmetry constraints is with 360 dimers centered between capsomers and the dimer dyad axes tangent to the viral surface (Fig. 4). This novel configuration would place all three glycans either near the outer surface of the EM density, or forming contacts with domain I from another dimer. The pattern formed by the G_C is strikingly similar to the distribution of the EM density of RVFV at an average radius of 47 nm (12) (Fig. 4). G_C occupies the inner half of the glycoprotein shell of RVFV, leaving density for the outer half of each capsomer vacant and available to accommodate G_N, as proposed by others (16). This would be consistent with alphavirus assemblies, in which the fusion protein E1 is covered by E2 (33, 34).

In the dimer-based assembly model (Fig. 4), domains I, II, and III contribute a different fraction of the surface of G_C at each of the four different types of capsomers in the $T = 12$ lattice. Thus, G_N would have to recognize distinct surfaces of G_C, albeit with similar (slightly negative) electrostatic potentials (Fig. S5). Furthermore, this model requires a degree of flexibility within the 41-residue stem region of G_C that connects the ectodomain to the transmembrane anchor (Fig. S1B), as the C terminus of domain III in one subunit within each G_C dimer is 40–50 Å away from the membrane (Fig. S3). For these reasons, conventional quasiequivalent icosahedral assemblies with monomeric G_C as the repeating unit, as proposed in a recent modeling study (16), remain plausible. In this case, the G_C dimer may still exist in intermediates of
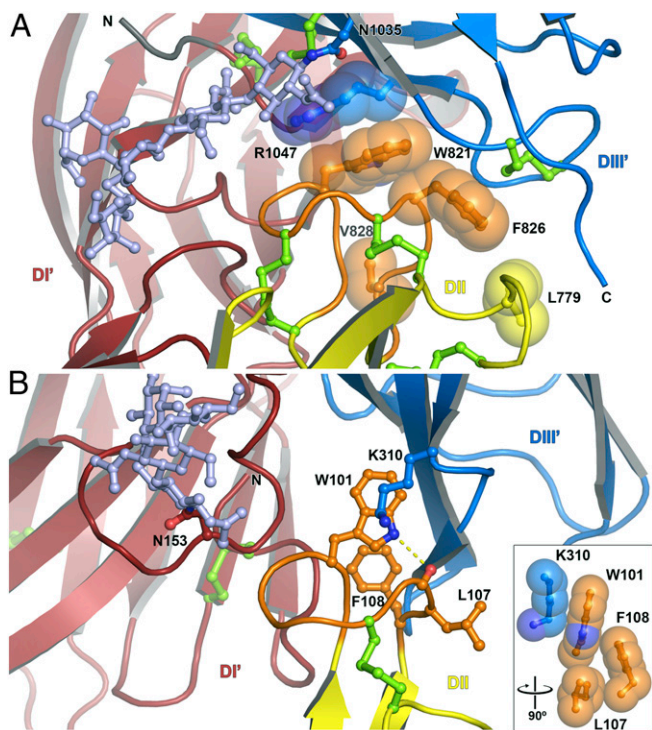
Fig. 3. Dimer contacts involving the fusion loops of RVFV G_C and dengue type 2 E. (*A*) In the RVFV G_C dimer interface, Trp821 in the fusion loop forms a π-stacking interaction with Arg1047 in domain III of the dimer partner (DIII'). The other side of the Trp821 side chain is packed against Phe826. (*B*) In the dengue type 2 E dimer interface, the Trp101 side chain forms a hydrogen bond with the main chain carbonyl oxygen of Leu107. (*Inset*) The hydrophobic interaction of Trp101 with Lys310 in domain III of the dimer partner (DIII').

membrane fusion or virus maturation that have not yet been observed by EM. The correlation of the G_C dimer-based model after fitting of the G_C icosahedral lattice into the EM density with UCSF Chimera (35) was 0.77. The fitting strategy is described in *Materials and Methods*, and complete quality-of-fit statistics are provided in Table S1. For comparison, the correlation of a monomer-based model with 12 G_N–G_C heterodimers was 0.80 (16). Although the correlations of the dimer- and monomer-based models are similar, the two numbers are not directly comparable because the dimer-based model lacks G_N, whereas the monomer-based assembly was generated using theoretical atomic models of G_N and G_C (and because different EM densities, fitting strategies, and software packages were used). In conclusion, various modes of G_C assembly remain possible, and EM data of RVFV at higher resolution or a crystal structure of G_N are necessary to definitively determine the organization of the glycoproteins within the virions.

Materials and Methods

Protein Expression and Purification. Genes encoding the ectodomain of G_C (G_C-ECD, M segment residues 691–1,159 or soluble G_C (sG_C, residues 691–1,119), followed by a C-terminal eight-histidine purification tag, were amplified from the M segment cDNA of RVFV the Egyptian (Sharqiya) ZH-548 strain (GenBank accession no. ABD38819.1) and subcloned into the pAcGP67 vector (BD Biosciences) in frame with the baculovirus gp67 signal sequence. Sf9 insect cells (Invitrogen) were cotransfected with one of the G_C expression constructs and Sapphire baculovirus genomic DNA (Allele Biotechnology) to produce recombinant baculoviruses expressing G_C-ECD or sG_C. Virus stocks were amplified with three sequential infections of Sf9 cells. For G_C expression, *Tni* insect cells (Expression Systems) grown at 27 °C were infected at a density of 3×10^6 cells/mL with 0.5% (vol/vol) of third-passage (P3) baculovirus stock. After culture in suspension for 96–105 h at 20 °C the culture media was collected, its pH was adjusted with 20 mM Tris·HCl pH 8. G_C-ECD was not secreted and could not be solubilized with detergents. sG_C was purified by nickel affinity chromatography with Ni-NTA agarose (Qiagen) followed by

size-exclusion chromatography with a Superdex 200 (10/300) GL column (GE Healthcare). The histidine tag was removed with carboxypeptidase A treatment at 16 °C for 16 h (1 milliunit/µg of G_C). Carboxypeptidase A was then inhibited with 1 mM EDTA and separated from cleaved sG_C by size-exclusion chromatography. To obtain nonglycosylated sG_C, 0.4 g/L tunicamycin was added to the growing culture upon baculovirus infection and sG_C was purified as described above. Protein samples were concentrated to 4.5–6 g/L, frozen in liquid nitrogen, and stored at −80 °C in 10 mM Tris pH 8, 0.1 M NaCl.

Hydrodynamic and Multiangle Scattering Analysis. Analytical size-exclusion chromatography and multiangle light scattering (MALS) experiments were performed in 50 mM NaOAc pH 5.0, MES pH 6.2, or Tris·HCl pH 8.0 and 0.1 M NaCl. A total of 0.1 mL sGC at 1 g/L was loaded onto a Superdex 200 (10/300) column coupled to a DAWN EOS spectrometer and OPTILAB DSP interferometric refractometer (Wyatt Technology) at a flow rate of 0.5 mL/min. sGC was detected as it eluted from the column with a UV detector at 280 nm, a light scattering detector at 690 nm, and a refractive index detector. The molar mass of sGC was determined from the Debye plot of light scattering intensity versus scattering angle. Data processing was performed with ASTRA software (Wyatt Technology).

Crystallization and Structure Determination of sG_C. Crystals of sG_C were grown by hanging drop vapor diffusion at 16 °C. sG_C at 4–6 g/L in 10 mM Tris pH 8.0, 0.1 M NaCl, 1.8 mM undecyl-β-D-maltoside (UDM) was mixed with a half volume of reservoir solution: 20% (wt/vol) polyethylene glycol 5000 methyl ether (PEG 5000 MME), 0.1 M sodium citrate pH 6.2, 0.1 M ammonium sulfate. After 3–4 d, crystal clusters were crushed and used as microseeds in drops preequilibrated for 6 h in 18% (wt/vol) PEG 5000 MME, 0.1 M MES pH 6.2, 0.1 M ammonium
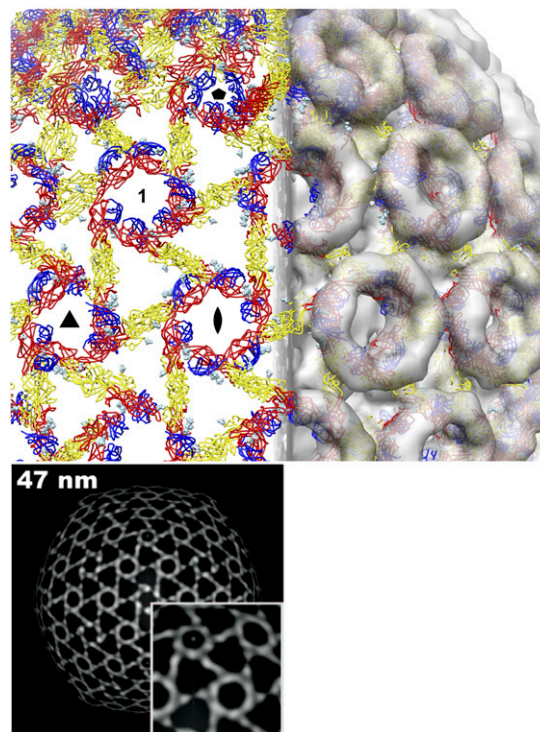

Fig. 4. Possible organization of the G_C dimer in the outer protein shell of RVFV. Six glycosylated G_C dimers fit into an asymmetric unit of the EM structure of RVFV (EMDataBank code EMD-1550) without major steric clashes and within the icosahedral symmetry constraints. In this configuration, 360 dimers (colored as in Fig. 2) are centered between capsomers, with the dimer dyad axes tangent to the viral surface. The glycans (light blue spheres) are either near the outer surface of the EM density or form contacts with another dimer. The G_C lattice occupies the inner half of the glycoprotein shell. A set of two-, three-, and fivefold icosahedral symmetry axes is labeled with standard symbols. The capsomer not centered on a symmetry axis is labeled "1." *Lower*, density distribution from an electron microscopy image reconstruction on a virus-shaped surface with an average radius of 47 nm. Reproduced with permission from American Society for Microbiology (12).

sulfate, 5% (vol/vol) glycerol, 1.8 mM UDM. Rod-shaped crystals reached a size of 200 × 50 × 50 μm in 2–3 wk and belonged to space group $P2_1$. Crystals were frozen in liquid nitrogen in reservoir solution supplemented with 25% glycerol (vol/vol) as a cryoprotectant. Crystals were derivatized by soaking in reservoir solution plus 1 mM $K_2[OsO_2(OH)_4]_2$ for 96 h. Nonglycosylated sG_C crystallized under the same crystallization solution condition except with a lower concentration of PEG 5000 MME (12–13%, wt/vol). Bipyramidal crystals of nonglycosylated sG_C grew up to 150 × 80 × 60 μm within 2 wk and belonged to space group $P6_422$. Data were collected at 100 K on a PILATUS detector (Dectris) and processed with XDS (36) and HKL2000 (37). The structure of glycosylated sG_C was determined by single-wavelength anomalous diffraction (SAD) with PHENIX (38). The atomic coordinates for domains I and II built with PHENIX were used as a molecular replacement search model with the highest resolution (1.9 Å) native data set. The atomic model was completed with COOT (39) and refined to an R_{free} of 25.6% with PHENIX and REFMAC (40). The structure of nonglycosylated sG_C was determined by molecular replacement using domains I and II of sG_C as separate search models. The position of domain III was determined using a spherically averaged phased translation function (41). Atomic coordinates and structure factors have been deposited in the Protein Data Bank (PDB ID codes 4HJ1 and 4HJC). See Table 1 for data collection and refinement statistics.

Fitting of the sG$_C$ Structure into the Electron Microscopy Structure. Six dimers of glycosylated sG_C were manually fitted into the EM image reconstruction of RVFV (EMDataBank ID code EMD-1550) (12) with UCSF Chimera (35). The positions of individual dimers in the resulting $T = 12$ icosahedral asymmetric unit were adjusted to remove major steric clashes and to optimize the fit into the density. At the contour level of 1.6 σ used for the manual fitting, the volume of the outer protein shell in the EM density was consistent with the molecular mass of 720 G_N–G_C heterodimers (~70 MDa), as would be expected for an icosahedral asymmetric unit with twelve G_N–G_C heterodimers.

The icosahedral asymmetric unit of G_C was then fitted with UCSF Chimera to optimize the correlation between the EM map and a map calculated at 20-Å resolution from the atomic coordinates of the asymmetric unit. Because G_N is assumed to be located in the distal ends of the capsomers and its structure is unknown, fitting of G_C was performed using an EM density map in which points outside of the 20-Å calculated map were set to zero, or "masked" out. This had the effect of restraining G_C to the inner half of the protein shell. Icosahedral symmetry was applied to the calculated map to generate the symmetry-related asymmetric units, and the 60 resulting asymmetric units were fit into the masked EM map with icosahedral symmetry enforced. Each of the six dimers within one asymmetric unit was then fitted sequentially, after subtracting the density corresponding to the other dimers within the asymmetric unit and in the adjacent symmetry-related asymmetric units. A second cycle of symmetry-enforced fitting was then performed as described above. The mask applied to the EM density was then expanded in all directions with a 3-Å "pad," to release the restraint on the radial position of G_C somewhat, and the entire fitting procedure described above (two symmetry-enforced fitting cycles separated by one sequential fitting cycle) was repeated with the expanded masked EM map. Correlations between the calculated map and the EM map (unmasked or masked) were calculated and are reported, along with other fitting statistics, in Table S1. The final correlation between the fitted map (calculated from the atomic coordinates) and the unmasked experimental EM map was 0.772.

1. Schmaljohn CS, Nichol ST (2007) Bunyaviridae. *Fields Virology*, eds Knipe DM, Howley PM (Lippincott Williams & Wilkins, Philadelphia), 5th Ed, Vol 2, pp 1741–1788.
2. Swanepoel R, Coetzer JAW (1994) Rift Valley fever. *Infectious Diseases of Livestock: With Special Reference to Southern Africa*, eds Coetzer JAW, Thomson GR, Tustin RC, Kriek NPJ (Oxford Univ Press, Cape Town), pp 688–717.
3. Gargan TP, 2nd, Clark GG, Dohm DJ, Turell MJ, Bailey CL (1988) Vector potential of selected North American mosquito species for Rift Valley fever virus. *Am J Trop Med Hyg* 38(2):440–446.
4. Enserink M (2008) Entomology. A mosquito goes global. *Science* 320(5878):864–866.
5. Stone R (2010) Infectious diseases. Rival teams identify a virus behind deaths in central China. *Science* 330(6000):20–21.
6. McMullan LK, et al. (2012) A new phlebovirus associated with severe febrile illness in Missouri. *N Engl J Med* 367(9):834–841.
7. Skehel JJ, Wiley DC (2000) Receptor binding and membrane fusion in virus entry: the influenza hemagglutinin. *Annu Rev Biochem* 69:531–569.
8. Modis Y, Ogata S, Clements D, Harrison SC (2004) Structure of the dengue virus envelope protein after membrane fusion. *Nature* 427(6972):313–319.
9. Gibbons DL, et al. (2004) Conformational change and protein-protein interactions of the fusion protein of Semliki Forest virus. *Nature* 427(6972):320–325.
10. Lozach PY, et al. (2010) Entry of bunyaviruses into mammalian cells. *Cell Host Microbe* 7(6):488–499.
11. Sherman MB, Freiberg AN, Holbrook MR, Watowich SJ (2009) Single-particle cryo-electron microscopy of Rift Valley fever virus. *Virology* 387(1):11–15.
12. Huiskonen JT, Overby AK, Weber F, Grünewald K (2009) Electron cryo-microscopy and single-particle averaging of Rift Valley fever virus: Evidence for GN-GC glycoprotein heterodimers. *J Virol* 83(8):3762–3769.
13. Liu L, Celma CC, Roy P (2008) Rift Valley fever virus structural proteins: Expression, characterization and assembly of recombinant proteins. *Virol J* 5:82.
14. Zheng F, et al. (2007) Defining the N-linked glycosylation site of Hantaan virus envelope glycoproteins essential for cell fusion. *J Microbiol* 45(1):41–47.
15. Garry CE, Garry RF (2004) Proteomics computational analyses suggest that the carboxyl terminal glycoproteins of Bunyaviruses are class II viral fusion protein (beta-penetrenes). *Theor Biol Med Model* 1:10.
16. Rusu M, et al. (2012) An assembly model of rift valley Fever virus. *Front Microbiol* 3:254.
17. Tischler ND, Gonzalez A, Perez-Acle T, Rosemblatt M, Valenzuela PD (2005) Hantavirus Gc glycoprotein: evidence for a class II fusion protein. *J Gen Virol* 86(Pt 11):2937–2947.
18. Gonzalez-Scarano F, Janssen RS, Najjar JA, Pobjecky N, Nathanson N (1985) An avirulent G1 glycoprotein variant of La Crosse bunyavirus with defective fusion function. *J Virol* 54(3):757–763.
19. Lescar J, et al. (2001) The fusion glycoprotein shell of Semliki Forest virus: An icosahedral assembly primed for fusogenic activation at endosomal pH. *Cell* 105(1):137–148.
20. Rey FA, Heinz FX, Mandl C, Kunz C, Harrison SC (1995) The envelope glycoprotein from tick-borne encephalitis virus at 2 A resolution. *Nature* 375(6529):291–298.
21. Modis Y, Ogata S, Clements D, Harrison SC (2003) A ligand-binding pocket in the dengue virus envelope glycoprotein. *Proc Natl Acad Sci USA* 100(12):6986–6991.

22. Holm L, Kääriäinen S, Rosenström P, Schenkel A (2008) Searching protein structure databases with DaliLite v.3. *Bioinformatics* 24(23):2780–2781.
23. Fritz R, Stiasny K, Heinz FX (2008) Identification of specific histidines as pH sensors in flavivirus membrane fusion. *J Cell Biol* 183(2):353–361.
24. Nayak V, et al. (2009) Crystal structure of dengue virus type 1 envelope protein in the postfusion conformation and its implications for membrane fusion. *J Virol* 83(9):4338–4344.
25. Qin ZL, Zheng Y, Kielian M (2009) Role of conserved histidine residues in the low-pH dependence of the Semliki Forest virus fusion protein. *J Virol* 83(9):4670–4677.
26. Zheng Y, Sánchez-San Martín C, Qin ZL, Kielian M (2011) The domain I-domain III linker plays an important role in the fusogenic conformational change of the alphavirus membrane fusion protein. *J Virol* 85(13):6334–6342.
27. de Boer SM, et al. (2012) Acid-activated structural reorganization of the rift valley Fever virus gc fusion protein. *J Virol* 86(24):13642–13652.
28. Chan DC, Kim PS (1998) HIV entry and its inhibition. *Cell* 93(5):681–684.
29. Allison SL, et al. (1995) Oligomeric rearrangement of tick-borne encephalitis virus envelope proteins induced by an acidic pH. *J Virol* 69(2):695–700.
30. Kanai R, et al. (2006) Crystal structure of West Nile virus envelope glycoprotein reveals viral surface epitopes. *J Virol* 80(22):11000–11008.
31. Luca VC, AbiMansour J, Nelson CA, Fremont DH (2012) Crystal structure of the Japanese encephalitis virus envelope protein. *J Virol* 86(4):2337–2346.
32. Kuhn RJ, et al. (2002) Structure of dengue virus: Implications for flavivirus organization, maturation, and fusion. *Cell* 108(5):717–725.
33. Li L, Jose J, Xiang Y, Kuhn RJ, Rossmann MG (2010) Structural changes of envelope proteins during alphavirus fusion. *Nature* 468(7324):705–708.
34. Voss JE, et al. (2010) Glycoprotein organization of Chikungunya virus particles revealed by X-ray crystallography. *Nature* 468(7324):709–712.
35. Pettersen EF, et al. (2004) UCSF Chimera—a visualization system for exploratory research and analysis. *J Comput Chem* 25(13):1605–1612.
36. Kabsch W (2010) XDS. *Acta Crystallogr D Biol Crystallogr* 66(Pt 2):125–132.
37. Otwinowski Z, Minor W (1997) Processing of X-ray diffraction data collected in oscillation mode. *Methods Enzymol* 276:307–326.
38. Adams PD, et al. (2002) PHENIX: Building new software for automated crystallographic structure determination. *Acta Crystallogr D Biol Crystallogr* 58(Pt 11):1948–1954.
39. Emsley P, Cowtan K (2004) Coot: Model-building tools for molecular graphics. *Acta Crystallogr D Biol Crystallogr* 60(Pt 12 Pt 1):2126–2132.
40. Murshudov GN, Vagin AA, Dodson EJ (1997) Refinement of macromolecular structures by the maximum-likelihood method. *Acta Crystallogr D Biol Crystallogr* 53(Pt 3):240–255.
41. Vagin AA, Isupov MN (2001) Spherically averaged phased translation function and its application to the search for molecules and fragments in electron-density maps. *Acta Crystallogr D Biol Crystallogr* 57(Pt 10):1451–1456.
42. Holm L, Rosenström P (2010) Dali server: Conservation mapping in 3D. *Nucleic Acids Res* 38(Web Server issue):W545–W549.

BIOPHYSICS AND COMPUTATIONAL BIOLOGY